ARMY RESEARCH LABORATORY

Simulated Thermal Spectro-polarimetric Signatures of Water and Dark-painted Objects in Various Environmental Conditions

by Melvin Felton

ARL-TR-5777 **September 2011**

NOTICES

Disclaimers

The findings in this report are not to be construed as an official Department of the Army position unless so designated by other authorized documents.

Citation of manufacturer's or trade names does not constitute an official endorsement or approval of the use thereof.

Destroy this report when it is no longer needed. Do not return it to the originator.

Army Research Laboratory
Adelphi, MD 20783-1197

ARL-TR-5777 **September 2011**

Simulated Thermal Spectro-polarimetric Signatures of Water and Dark-painted Objects in Various Environmental Conditions

Melvin Felton
Computational and Information Sciences Directorate, ARL

REPORT DOCUMENTATION PAGE

Form Approved
OMB No. 0704-0188

1. REPORT DATE *(DD-MM-YYYY)*	2. REPORT TYPE	3. DATES COVERED (From - To)
September 2011	Summary	

4. TITLE AND SUBTITLE
Simulated Thermal Spectro-polarimetric Signatures of Water and Dark-painted Objects in Various Environmental Conditions

5a. CONTRACT NUMBER

5b. GRANT NUMBER

5c. PROGRAM ELEMENT NUMBER

6. AUTHOR(S)
Melvin Felton

5d. PROJECT NUMBER

5e. TASK NUMBER

5f. WORK UNIT NUMBER

7. PERFORMING ORGANIZATION NAME(S) AND ADDRESS(ES)
U.S. Army Research Laboratory
ATTN: RDRL-CIE-S
2800 Powder Mill Road
Adelphi, MD 20783-1197

8. PERFORMING ORGANIZATION REPORT NUMBER
ARL-TR-5777

9. SPONSORING/MONITORING AGENCY NAME(S) AND ADDRESS(ES)

10. SPONSOR/MONITOR'S ACRONYM(S)

11. SPONSOR/MONITOR'S REPORT NUMBER(S)

12. DISTRIBUTION/AVAILABILITY STATEMENT
Approved for public release; distribution unlimited.

13. SUPPLEMENTARY NOTES

14. ABSTRACT
The research presented in this report aims at elucidating the environmental factors that affect the spectro-polarimetric signatures of water and a dark-painted surface outdoors. We highlight the importance of thermal contrast between the object of interest and its optical background; explicitly present the analysis for four environmental scenarios (clear sky and dry atmosphere, clear sky and humid atmosphere, altostratus clouds, and cumulus clouds); and for each scenario, present the angular dependence of the degree of linear polarization for various band-averages within the two infrared (IR) imaging windows (3–5 and 8–12 μm). It is shown that midwave IR (MWIR) polarimetric contrast between an object and its visible background in a scene can be reduced in clear sky conditions due to the competing components of reflected solar radiance and radiance emitted from the object while the same contrast may be increased when cloudy conditions nullify the scattered solar radiance. In addition, long-wave IR (LWIR) polarimetric contrast is highest for clear sky conditions and may be reduced as the contribution from the optical background increases.

15. SUBJECT TERMS
Thermal imaging, polarimetric imaging, target contrast

16. SECURITY CLASSIFICATION OF:			17. LIMITATION OF ABSTRACT	18. NUMBER OF PAGES	19a. NAME OF RESPONSIBLE PERSON
a. REPORT	b. ABSTRACT	c. THIS PAGE			Melvin Felton
Unclassified	Unclassified	Unclassified	UU	18	19b. TELEPHONE NUMBER (*Include area code*) (301) 394-2618

Contents

List of Figures

1. Introduction

The physical quantities associated with light that are relevant for environmental sensing are intensity, wavelength, and polarization. Average intensities within a relatively wide infrared (IR) waveband (generally, 3–5 and 8–12 μm) are used in conventional thermal imaging, which is used extensively in today's modern military applications. Both the spectral and polarization information in the IR light forming the image of a scene can be used to enhance conventional thermal imaging. Spectral imagers increase the number of wavebands by subdividing the IR imaging windows, which provides information about the materials that make up a scene. Imaging polarimetry measures the polarization of the light forming the image through filtering techniques, which provides information about the surface geometry and roughness of the objects in the scene. Because manmade objects have different geometrical and roughness features from that of the natural background, polarimetric imaging can be used as a discriminator between the two. This results in the reduction of "clutter" within polarimetric images, where clutter is defined as features of the natural background that show up in images and make it difficult to identify objects of interest. In addition, thermal polarimetric imaging does not need thermal contrast between an object and its visible background in the scene, and so therefore, may provide useful contrast during periods of low thermal contrast.

The sources of polarized IR light in a scene are due to emission and reflection. Light polarized due to pure emission is oriented in the plane defined by the surface normal and the observer's line of sight (LOS), while light that is polarized as a result of reflection is oriented perpendicular to the plane defined by the surface normal and the observer's LOS. In most situations, these to two opposing components exist simultaneously to varying degrees.

Because these two components are orthogonal, their superposition results in a net reduction of the overall magnitude of the polarimetric signature of an object. The sources of ambient IR radiation that may or may not be visible within the scene but still illuminate the objects in the field of view of the camera are referred to as the optical background (*1*). The temperature of an object affects the overall polarimetric signature in as much as it serves to increase or decrease the magnitude of the emission component of the overall polarization state.

The factors that affect the resultant polarization signature of an object are the effective temperature differences between it and its optical background and its reflective and emissive properties. The most important of these factors is the former, namely, the thermal contrast between the object and its optical background. For any object, the thermal contrast between it and its optical background leads to three polarimetric signature regimes: (1) reflection dominant when the optical background effective temperature is larger than the object effective temperature, (2) emission dominant when the object effective temperature is larger than the optical background effective temperature, and (3) no polarization when the two effective

temperatures are equal. The thermal polarimetric signature of objects in the midwave IR (MWIR) and long-wave IR (LWIR) wavebands (and sub-bands thereof) can be in different regimes simultaneously, or in other words, in the same environmental conditions.

The research presented in this report aims at elucidating the environmental factors that affect the spectro-polarimetric signatures of objects outdoors. The work of Joe Shaw (*2, 3*) is extended here to include more details of the thermal polarimetric signature of water outdoors and a similar analysis is performed for a dark painted surface (e.g., flat black paint). We highlight the importance of thermal contrast between the object of interest and its optical background; explicitly present the analysis for four environmental scenarios (clear sky and dry atmosphere, clear sky and humid atmosphere, altostratus clouds, and cumulus clouds); and for each scenario, present the angular dependence of the degree of linear polarization for various band-averages.

2. Model

The radiative transfer for the scenarios modeled in this study is presented in figure 1. The optical background in this case is defined as the constituents of the atmosphere that serve as sources of IR radiation in the 3–5 and 8–12 μm thermal imaging windows and includes aerosol and molecular emission, cloud emission, and scattered solar radiation. With the exception of some thin cirrus cloud emissions (not included in this study), these forms of radiation are unpolarized. This is depicted on the red arrow representing the optical background radiance where the black arrows are the emission component polarized parallel to the plane of the page (p-polarization) and the dots are the emission component polarized perpendicular to the plane of the page (s-polarization). When this radiation is reflected off of a smooth surface, it becomes completely polarized in the s-state. The surface itself emits radiation that is polarized in the p-state. In addition to this reflection and emission, there is also unpolarized emission from the atmospheric path between the imager and the surface. These three sources of radiation combine to form the net radiation observed by the imager.

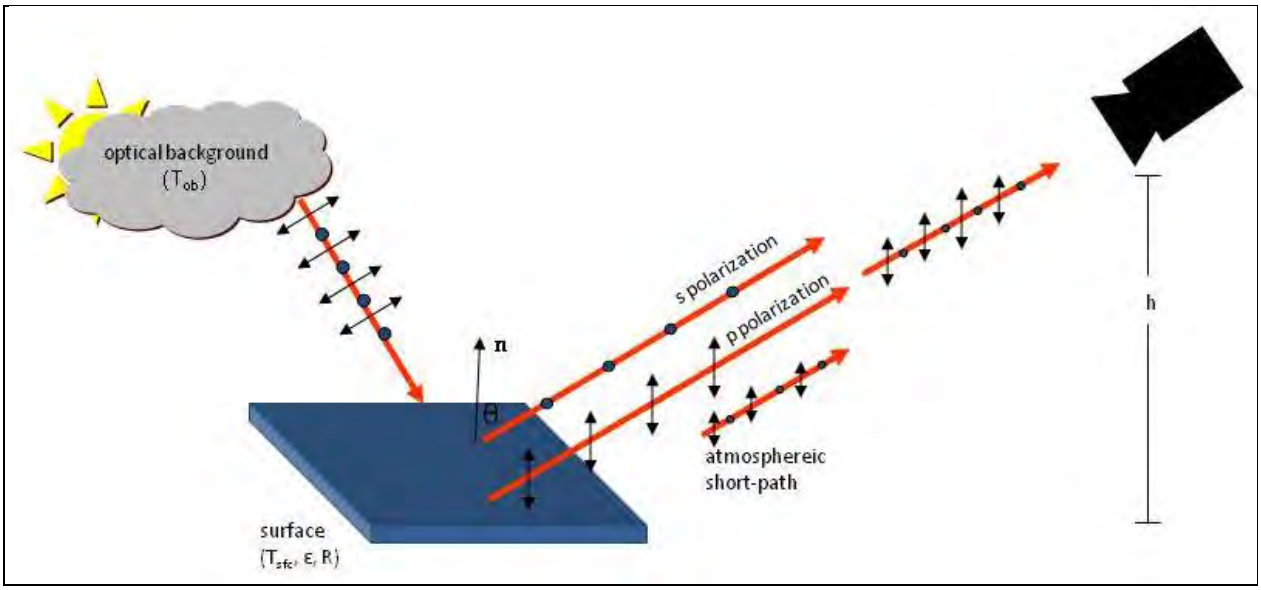

Figure 1. Radiative transfer for the scenarios modeled in this study. The net radiance observed by the imager is a superposition of reflected optical background radiation, surface emission from the target surface, and atmospheric short-path emission.

The net radiance in each polarization state, $L^{s,p}$, is calculated using equation 1. The "s" and "p" superscripts indicate s- and p-polarization, respectively. The absorption of the optical background and surface emissions (L_{ob} and L_{sfc}, respectively) by the atmospheric molecular species, such as water (H_2O), carbon dioxide (CO_2), and ozone (O_3), is accounted for by the atmospheric transmission, τ_{atm}. The radiance terms on the right-hand-side of equation 1 are calculated using the Plank function for T_{ob} and T_{sfc}. The surface emissive and reflective properties are accounted for by the emissivity, ε_{sfc}, and reflectivity, R_{sfc}, which are related by the expression in equation 2.

$$L^{s,p} = \tau_{atm}\varepsilon_{sfc}^{s,p}L_{sfc}^{s,p} + L_{atm} + \tau_{atm}R_{sfc}^{s,p}L_{ob} \quad (1)$$

$$\varepsilon_{sfc}^{s,p} = 1 - R_{sfc}^{s,p} \quad (2)$$

The reflectivity for the s- and p-polarization states is calculated using equations 3 and 4, respectively, and is a function of wavelength (λ) and incident angle (θ). The complex index of refraction is denoted by $\tilde{n}$ and the angle of refraction, θ_r, is expressed in terms of θ in equation 5.

$$R_{sfc}^{s}(\lambda,\theta) = \left|\frac{\cos(\theta)-\tilde{n}(\lambda)\cos(\theta_r)}{\cos(\theta)+\tilde{n}(\lambda)\cos(\theta_r)}\right|^2 \quad (3)$$

$$R_{sfc}^{p}(\lambda,\theta) = \left|\frac{\tilde{n}(\lambda)\cos(\theta)-\cos(\theta_r)}{\tilde{n}(\lambda)\cos(\theta)+\cos(\theta_r)}\right|^2 \quad (4)$$

$$\theta_r(\lambda,\theta) = \sin^{-1}\left[\frac{\sin(\theta)}{\tilde{n}(\lambda)}\right] \quad (5)$$

The degree of linear polarization (DOLP) can be calculated using the net radiance for each polarization state according to equation 6:

$$DOLP = \frac{L^s - L^p}{L^s + L^p} \quad (6)$$

The radiance terms used in this study are calculated using MODTRAN. A total of four environmental scenarios were modeled and arranged according to increasing magnitudes of the optical background radiation. These scenarios include clear sky and relatively dry atmosphere; clear sky and relatively humid atmosphere; altostratus clouds; and cumulus clouds. The 1976 U.S. Standard Atmosphere profile was used for all scenarios with the exception of the mid-Atlantic winter water vapor profile used for the clear and dry scenario and the mid-Atlantic summer water vapor profile used for the clear and humid scenario. Scattered solar radiance was included and a maritime aerosol model with 23-km visibility was used (*2, 3*). Other particulars of the MODTRAN settings include the use of the Henyey-Greenstein scattering phase function with an asymmetry factor of zero and the solar zenith and azimuth angles were set to 30° and 0°, respectively (*2*, *3*). The horizontal distance between the imager and the target object was held constant at 500 m and the viewing angle varied from 0°–85°.

3. Results

The results are presented in the form of a matrix of plots that allows for the comparison of spectral DOLP values calculated for a 75° viewing angle, thermal contrast between the optical background and target surface (L_{ob}-L_{sfc}) for a 75° viewing angle, and the angle dependence of band-averaged DOLP for all four environmental scenarios. The axes for the three types of plots remain the same for all four scenarios to allow comparison of the changes in their respective magnitudes. The sign of the spectral DOLP values indicates the polarization regime: negative for emission and positive for reflection. The two surface types examined in this study were assumed to be smooth and are water (288.15 K surface temperature) and a dark-painted surface (294.26 K surface temperature). The complex indices of refraction for water in the wavelength range 3–15 μm were obtained from Hale et al. (*4*), while the complex index of refraction used to characterize the dark-painted surface ($\tilde{n}$= 1.3 + 0.4i) was obtained from Schott (*5*). The graybody assumption was made for the dark-painted surface and the analysis was restricted to the 8–12 μm waveband since most military targets are close to graybodies for these wavelengths (*6*).

3.1 Water

The results of the simulation of the thermal polarimetric signature of water in the four environmental scenarios considered here are presented in figure 2. The thermal contrast between the optical background and the target surface is the highest during the “Clear and Dry” scenario

due to the low thermal emission of the cold sky. As a result, the majority of the polarized 3–15 µm image-forming light is polarized due to emission. The exception is between 3–3.6 µm, which is polarized due to the reflection of scattered solar radiation in that particular waveband. The band-averaged DOLP values for the reflection dominant 3–3.6 µm waveband reaches its maximum magnitude of approximately 8.5% at an 80° viewing angle. On the other hand, the band-averaged DOLP values for the emission-dominant 3.6–5 µm waveband reaches its maximum magnitude of just less than 3% at a viewing angle of 70°. When the entire MWIR waveband is considered, cancelation between reflection and emission components results in a maximum 3–5 µm band-averaged DOLP magnitude of <1% at 60°. The band-averaged LWIR (8–12 µm) DOLP reaches its maximum magnitude of just less than 6% at an 80° viewing angle.

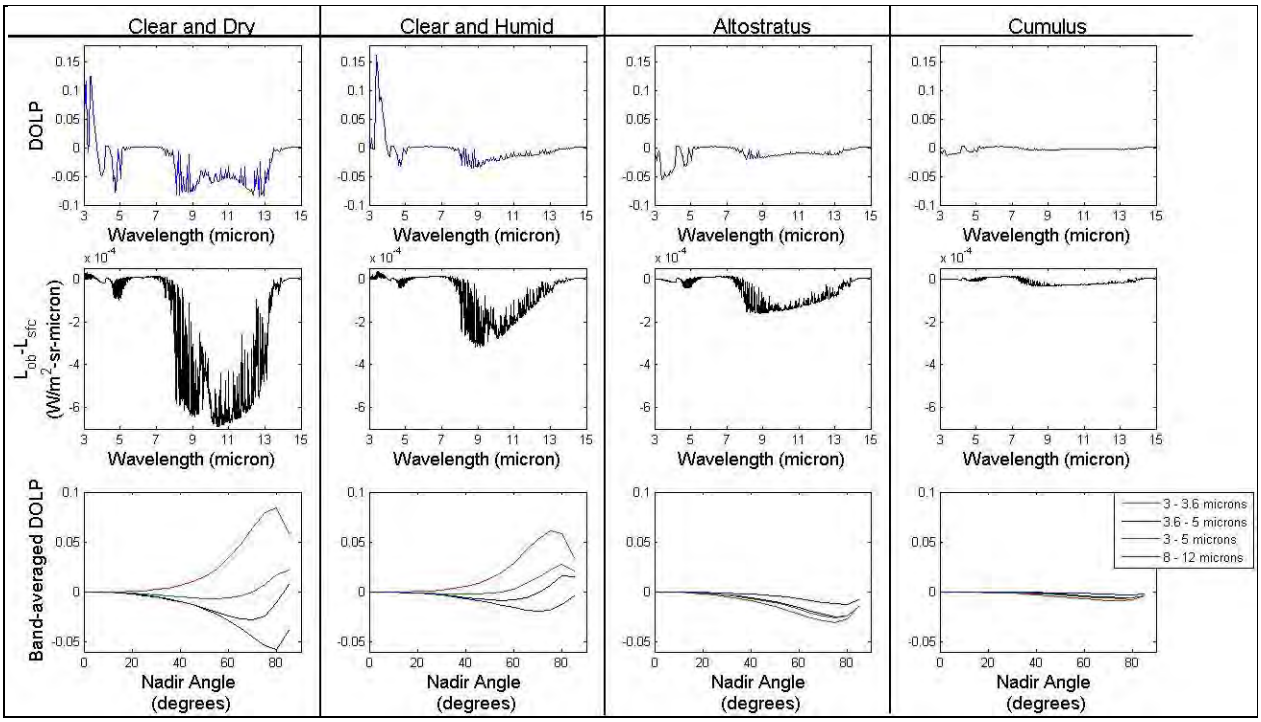

Figure 2. Spectral DOLP for a 75° viewing angle, thermal contrast between optical background and target surface (L_{ob}–L_{sfc}) at a 75° viewing angle, and the dependence of band-averaged DOLP on viewing angle for the polarimetric signature of water in all four environmental scenarios considered in this study.

In the "Clear and Humid" scenario, the extra water vapor in the atmosphere acts as an additional source of IR light in the optical background, resulting in an overall reduction in the emission-dominant polarization due to reduced thermal contrast between the optical background and target surface. There remains a component of the image-forming light that is polarized due to reflection of scattered solar radiation in the 3–3.6 µm waveband. Despite an overall reduction in magnitude, the general shape of the band-averaged DOLP values for the "Clear and Humid" scenario is similar to that of the "Clear and Dry" scenario.

The source of polarized image-forming IR light is greatly affected by the presence of clouds in the "Altostratus" scenario. The clouds shield the scene from scattered solar light in the 3–3.6 μm waveband, which eliminates the source of the image-forming light that was polarized upon reflection in the first two scenarios. As a result, the 3–3.6 μm image-forming light in this scenario is polarized due to emission. The thermal contrast between the optical background and target surface in the 3.6–5 μm waveband is similar to that in the "Clear and Humid" scenario, and so therefore, the magnitude of the spectral DOLP in this waveband is also similar to that of the "Clear and Humid" scenario. In the 8–12 μm waveband, the effect of clouds is a further reduction to the thermal contrast between the optical background and the target surface, resulting in a lower magnitude of spectral DOLP. The effect of the lower thermal contrast between optical background and target surface and the shielding of the scattered solar radiation can be seen in the band-averaged DOLP. Note that in the 3–3.6 μm waveband, the band-averaged DOLP, which in the previous scenarios had the highest magnitudes and was due to reflection, still has the highest magnitude but is now due to emission.

In the "Cumulus" scenario, there is a reduction in thermal contrast between optical background and target surface across both imaging windows, namely, 3–5 and 8–12 μm. This resulted in an overall reduction in the spectral and band-averaged DOLP magnitudes. Maximum values of band-averaged DOLP magnitude for the 3–3.6, 3.6–5, 3–5, and 8–12 μm wavebands are 1%, 0.5%, 0.6%, and 0.25%, respectively.

3.2 Dark-painted Surface

The results of the simulation of the thermal polarimetric signature of a dark-painted (e.g., flat black paint) surface in the four environmental scenarios considered here are presented in figure 3. The highest DOLP magnitudes are observed for the "Clear and Dry" scenario due to the high thermal contrast between the optical background and target surface. In this scenario, a peak band-averaged DOLP magnitude of 13% occurs at a 75° viewing angle.

For the three remaining scenarios, there is an increasing amount of ambient IR loading due to water vapor, altostratus clouds, and cumulus clouds, which reduces the thermal contrast between the optical background and the target surface in the "Clear and Humid," "Altostratus," and "Cumulus" scenarios, respectively, resulting in a reduction in spectral and band-averaged DOLP magnitudes.

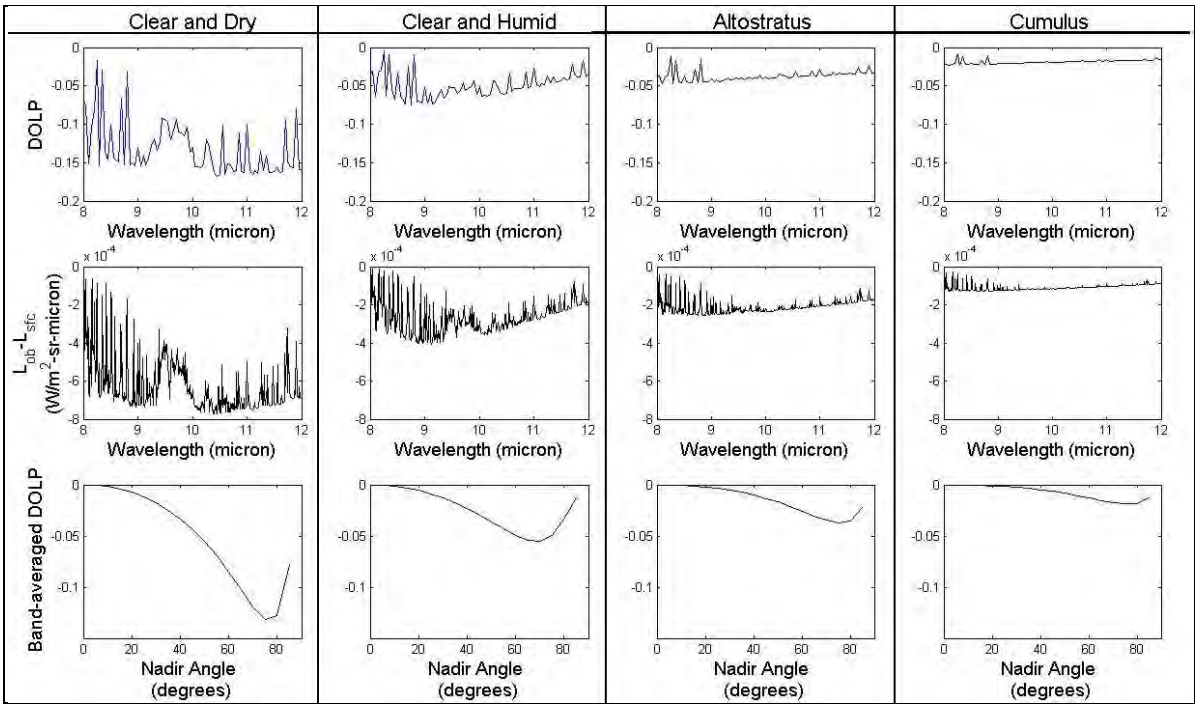

Figure 3. Spectral DOLP for a 75° viewing angle, thermal contrast between optical background and target surface (L_{ob}–L_{sfc}) for a 75° viewing angle, and the dependence of band-averaged DOLP on viewing angle for the polarimetric signature of a dark-painted surface in all four environmental scenarios considered in this study.

4. Conclusion

The results of this study are largely consistent with the findings in the literature concerning the nature of thermal polarimetric imaging of targets outdoors, namely, that LWIR polarimetric signatures are predominantly emission-dominant while the MWIR polarimetric signatures are due to a combination of emission and reflection (*7*). In addition, the lower the thermal contrast between a target and its optical background, the lower the magnitude of the polarimetric signature for that target. Moreover, we've seen that if solar scattering is blocked from reaching the scene being imaged because of, say, a cloud, then the MWIR polarimetric signatures will become emission-dominant. On the other hand, the results of this study indicate that LWIR polarimetric signatures may enter a reflection-dominant regime if the target surface at ambient temperature is highly reflective, such as unpainted metal, water, or glass; and there is strong IR loading onto the target from the optical background, such as low, thick cumulus clouds, which sometimes have temperatures on the order of the ambient surface temperature (*2, 3, 8*).

One of the ways in which thermal polarimetric imaging enhances conventional thermal imaging is through its ability to suppress the natural background. The mechanism behind this is the irregular surface features of the natural background, which may include grass, trees, bushes, etc.

The DOLP for such objects is usually on the order of <1%. With this knowledge, it can be inferred that contrast between a target and the natural background in a polarimetric image is typically lost when the target's DOLP is on the order of 1–2%. In this study, target DOLP values of this magnitude occurred during the "Clear and Dry" scenario for the 3–5 μm imaging window due to the cancelation between reflection and emission. These results indicate that improved MWIR polarimetric contrast can be achieved in a "Clear and Dry" scenario by imaging separately in the 3–3.6 μm (reflection-dominant) and 3.6–5 μm (emission-dominant) wavebands. This may result in a signal-to-noise problem since signals levels are already low when the entire MWIR imaging window is used to form a polarimetric image. When ambient IR loading is increased due to thermal emission from clouds, the magnitudes of both MWIR and LWIR polarimetric signatures are reduced. In these situations, though, there is no longer a cancelation effect taking place between reflection and emission in the MWIR imaging window. For this reason, MWIR DOLP magnitudes tend to be higher than LWIR DOLP magnitudes (by 1–2% in the "Altostratus" scenario), which may result in higher contrast between the target and the natural background in MWIR polarimetric images in cloudy conditions than the same contrast in LWIR polarimetric images.

The above conclusions concerning contrast within thermal polarimetric images have been observed experimentally (*9*, *10*). In particular, Felton et al. (*9*) presented results that showed improved MWIR polarimetric contrast between a surrogate tank and the natural background under cloudy conditions. The data indicated that under clear sky conditions, the surrogate tank's MWIR polarimetric signature was in an emission-dominant regime and when clouds entered the optical background, its signature transitioned to a reflection-dominant regime. This is at odds with the theoretical results presented in this study in which the scattered sunlight illuminating the scene results in polarized reflection while scattered sunlight-blocking clouds leads to emission-dominant polarization for the target being imaged. This discrepancy could be due to the definition of the MWIR S_1 Stokes image data product in the Felton et al. (*9*) study. There will be a sign reversal if S_1 is defined as vertical polarized light minus horizontal polarized light as opposed to horizontal minus vertical.

5. References

1. Tyo, J. S.; Ratliff, B. M.; Boger, J. K.; Black, W. T.; Bowers, D. L.; Fetrow, M. P. The Effects of Thermal Equilibrium and Contrast in LWIR Polarimetric Images. *Optics Exp.* **2007**, *15* (23), 15161–15167.

2. Shaw, J. A. Degree of Linear Polarization in Spectral Radiances from Water-viewing Infrared Radiometers. *App. Optics* **1999**, *38* (15), 3157–3156.

3. Shaw, J. A. A Survey of Infrared Polarization in the Outdoors. *Proc. of SPIE*, 6660, 2007.

4. Hale, G. M.; Querry, M. R. Optical Constants of Water in the 200-nm to 200-μm Wavelength Region. *App. Optics* **1973**, *12* (3), 555–563.

5. Schott, J. R. *Fundamentals of Polarimetric Remote Sensing*. SPIE Press, Bellingham, Washington USA, 2009, 225.

6. Shumaker, D. L.; Wood, J. T.; Thacker, C. R. *Infrared Imaging Systems Analysis*, DCS Corporation, Alexandria, VA, 1993, 2-49.

7. Tyo, J. S.; Goldstein, D. L.; Chenault, D. B.; Shaw, J. A. Review of Passive Imaging Polarimetry for Remote Sensing Applications. *App. Optics* **2006**, *45* (22), 5453–5469.

8. Shaw, J. A.; Nugent, P. W.; Pust, N. J.; Thurairajah, B. Radiometric Cloud Imaging with an Uncooled Microbolometer Thermal Infrared Camera. *Optics Exp.* **2005**, *13* (15), 5807–5817.

9. Felton, M.; Gurton, K. P.; Pezzaniti, J. L.; Chenault, D. B.; Roth, L. E. Measured Comparison of the Crossover Periods for Mid- and Long-wave IR (MWIR and LWIR) Polarimetric and Conventional Thermal Imagery. *Optics Exp.* **2010**, *18* (15), 15704–15713.

10. McCarthy, J.; Woolley, M.; Roth, L. Correlation of Environmental Data Measurements with Polarimetric LWIR Sensor Measurements of Manmade Objects in Natural Clutter. *Proc. SPIE*, 7672, 2010.

List of Symbols, Abbreviations, and Acronyms

CO_2	carbon dioxide
DOLP	degree of linear polarization
H_2O	water
IR	infrared
LOS	line of sight
LWIR	long-wave IR
MWIR	midwave IR
O_3	ozone

1 (PDF only) DEFENSE TECHNICAL INFORMATION CTR
DTIC OCA
8725 JOHN J KINGMAN RD
STE 0944
FORT BELVOIR VA 22060-6218

1 DIRECTOR
US ARMY RESEARCH LAB
IMNE ALC HRR
2800 POWDER MILL RD
ADELPHI MD 20783-1197

1 DIRECTOR
US ARMY RESEARCH LAB
RDRL CIO LL
2800 POWDER MILL RD
ADELPHI MD 20783-1197

1 DIRECTOR
US ARMY RESEARCH LAB
RDRL CIO MT
2800 POWDER MILL RD
ADELPHI MD 20783-1197

1 DIRECTOR
US ARMY RESEARCH LAB
RDRL D
2800 POWDER MILL RD
ADELPHI MD 20783-1197

1 DIRECTOR
US ARMY RESEARCH LAB
RDRL CIE S M FELTON
2800 POWDER MILL RD
ADELPHI MD 20783-1197

3 US ARMY RDECOM ARDEC
ATT AMSRD AAR MEF S
LE ROTH
ATTN M WOOLLEY
ATTN AMSRD AAR AEP S
J ROMANO
BLDG 407
PICATINNY ARSENAL NJ
07806-5000

1 AFRL/RYJT
ATTN D PERRY
2241 AVIONICS CIRCLE BLDG 620
WRIGHT-PATTERSON AFB OH
45433-7320

INTENTIONALLY LEFT BLANK.